




Regionless Explicit Model Predictive Control of Active Suspension Systems With Preview

Johan Theunissen, Aldo Sorniotti , Member, IEEE, Patrick Gruber , Saber Fallah , Marco Ricco, Michal Kvasnica, and Miguel Dhaens

Abstract—Latest advances in road profile sensors make the implementation of preemptive suspension control a viable option for production vehicles. From the control side, model predictive control (MPC) in combination with preview is a powerful solution for this application. However, the significant computational load associated with conventional implicit model predictive controllers is one of the limiting factors to the widespread industrial adoption of MPC. As an alternative, this article proposes an explicit model predictive controller (e-MPC) for an active suspension system with preview. The MPC optimization is run offline, and the online controller is reduced to a function evaluation. To overcome the increased memory requirements, the controller uses the recently developed regionless e-MPC approach. The controller is assessed through simulations and experiments on a sport utility vehicle demonstrator with controllable hydraulic suspension actuators. For frequencies <4 Hz, the experimental results with the regionless e-MPC without preview show a $\sim 10\%$ reduction of the root-mean-square (RMS) value of the vertical acceleration of the sprung mass with respect to the same vehicle with a skyhook controller. In the same frequency range, the addition of preview improves the heave and pitch acceleration performance by a further 8 to 21%.

Index Terms—Active suspension, preview, regionless explicit model predictive control, ride comfort.

I. INTRODUCTION

THE performance benefits of active suspension systems that account for the road profile ahead have been investigated and demonstrated by several authors ([1]–[4]). Preview strategies for controllable suspensions are typically based on a feedforward disturbance compensation and a state feedback contribution. An industrial benchmark is the integrated

Manuscript received November 19, 2018; revised February 21, 2019 and May 1, 2019; accepted June 6, 2019. Date of publication July 12, 2019; date of current version February 10, 2020. This work was supported in part by Tenneco Automotive Europe and in part by the Slovak Research and Development Agency (Projects APVV 15-0007 and VEGA 1/0585/19). (Corresponding author: Aldo Sorniotti.)

J. Theunissen is with Simmanco, 3060 Korbeek-Dijle, Belgium (e-mail: johan.theunissen@simmanco.com).

A. Sorniotti, P. Gruber, S. Fallah, and M. Ricco are with the University of Surrey, Guildford GU2 7XH, U.K. (e-mail: a.sorniotti@surrey.ac.uk; p.gruber@surrey.ac.uk; s.fallah@surrey.ac.uk; m.ricco@surrey.ac.uk).

M. Kvasnica is with the Slovak University of Technology, 811 07 Bratislava, Slovakia (e-mail: michal.kvasnica@stuba.sk).

M. Dhaens is with Tenneco Automotive Europe BVBA, 3800 Sint-Truiden, Belgium (e-mail: mdhaens@Tenneco.com).

Color versions of one or more of the figures in this article are available online at <http://ieeexplore.ieee.org>.

Digital Object Identifier 10.1109/TIE.2019.2926056

TABLE I
REDUCTION (IN %) OF THE RMS VALUES OF THE HEAVE ACCELERATION, DUE TO MPC AND PREVIEW

Ref.	Susp. type	Compared to the passive set-up		Compared to another controller type		
		MPC w/o preview	MPC w/ preview	Ctrl. type	MPC w/o preview	MPC w/ preview
[22]	Active	n.a.	25 – 60%	Skyhook/ LQR	n.a.	n.a.
[23]	Active	37 – 38 %	43%		0 – 15%	7 – 20%
[24]	Semiactive	n.a.	n.a.	Skyhook	18%	40%
[25]	Active	n.a.	28%	Skyhook	n.a.	20%
[26]	Semiactive	n.a.	14%	LQR + preview	n.a.	n.a.
[27]	Leveling	n.a.	40 – 90%		n.a.	10 – 73%
[28]	Leveling	n.a.	> 50%	LQR	n.a.	n.a.
[36]	Semiactive	n.a.	n.a.		< 5%	n.a.

Note: Only [23] includes a comparison based on experimental results.

feedforward-feedback scheme by Mercedes-Benz for ride height adjustment through hydraulic active suspension actuators ([5], [6]).

A wide range of preview suspension controllers has been proposed in the literature, including feedforward compensators [7], fuzzy logic controllers [8], gain scheduled controllers [9], and neural network implementations [10]. Linear quadratic regulators (LQRs) and linear quadratic Gaussian controllers are frequently adopted optimal control strategies for preview suspensions, because of their simple formulations and the common assumption of linear suspension dynamics ([11]–[17]). H_∞ and H_2/H_∞ controllers can deal with model uncertainties, external disturbances and parameter variations, e.g., the sprung mass variation depending on the vehicle load condition ([18]–[21]).

The idea of accounting for future disturbances from the road ahead and for system or actuator constraints fits well with the model predictive control (MPC) philosophy. Hence, several authors, e.g., [22]–[31], proposed MPC implementations for preview suspension systems. Table I indicates the ride comfort benefits of various MPC suspension control implementations from the literature without and with preview, with respect to the passive vehicle and the same vehicle with a more conventional controller, such as an LQR or skyhook. To the best of our knowledge, the published work to date focused on conventional implicit model predictive control (i-MPC) implementations, in which the optimization is run online. This, in turn, requires

significant computational power and makes industrial implementations relatively difficult. As a consequence, most of the studies are limited to simulation-based assessments. The very few papers with experimental results either use high-performance processors [24] or very long sample times, i.e., 30 ms [23], to allow real-time implementation of the controllers.

To facilitate the industrial adoption of MPC for active suspension control with preview, this article proposes an e-MPC approach ([32], [33]). With e-MPC the optimization problem is solved offline for an assigned range of operating conditions. The first output of the optimal control sequence is stored as an “explicit” function of the states, and the online algorithm is reduced to a simple function evaluation. Hence, e-MPC requires a limited amount of online computational power compared to i-MPC, while providing similar performance and ability to handle constraints. On the other hand, the challenges of e-MPC are the increased design complexity and memory requirements. The latter issue is significantly mitigated by the recently developed theory of regionless e-MPC ([34], [35]). Region-based e-MPCs—but not regionless e-MPCs—have already been implemented in simulation ([36]–[39]) on semiactive and active suspensions without preview. In a few cases, they have also been preliminarily experimentally validated ([40], [41]). However, to the best of the knowledge of the authors, e-MPC has not been proposed so far for preview suspension control.

In summary, the contributions of this article are as follows.

- 1) The e-MPC formulation for active suspension systems with preview.
- 2) The adoption of the regionless e-MPC approach for suspension control. This facilitates the implementation at shorter time steps with respect to i-MPC, and reduces the memory requirements in comparison with the traditional region-based e-MPC.

The proof-of-concept regionless e-MPC algorithm is assessed through vehicle simulations and preliminary experimental tests on a vehicle demonstrator equipped with four commercially available active suspension actuators.

II. INTERNAL MODEL FORMULATION

This article proposes a decentralized controller, i.e., based on an independent controller for each vehicle corner (see also Section III-D). As a consequence, a quarter car (QC) model (see Fig. 1) is used for the internal model of the MPC formulation

$$\begin{aligned} m_1 \ddot{x}_1 + k_1 (x_1 - x_2) + c_1 (\dot{x}_1 - \dot{x}_2) + u_a &= 0 \\ m_2 \ddot{x}_2 + k_1 (x_2 - x_1) + k_2 (x_2 - w_0) \\ + c_1 (\dot{x}_2 - \dot{x}_1) + c_2 (\dot{x}_2 - \dot{w}_0) - u_a &= 0 \end{aligned} \quad (1)$$

where u_a is the actual force generated by the actuator; m_1 and m_2 are the sprung and unsprung masses; k_1 and c_1 are the vertical suspension stiffness and residual damping of the passive components; k_2 and c_2 are tire stiffness and damping; x_1 and x_2 are the sprung and unsprung mass displacements; and w_0 is the vertical displacement of the tire contact patch. For simplicity, the implementation of this article assumes $c_2 \approx 0$.

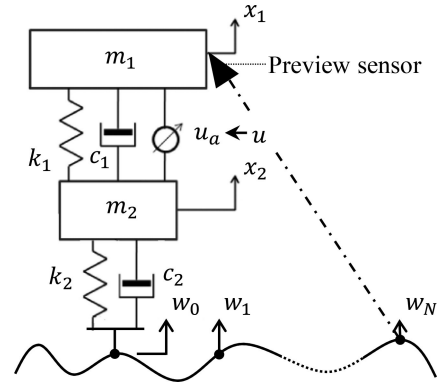


Fig. 1. QC model, including the hydraulic actuator, the road profile model and preview capability.

Usually, the main nonlinearity of a suspension system is due to the characteristic of the passive damper, which is absent in the specific plant. Moreover, the damping resulting from other passive suspension components (e.g., the bushings) is very small, so that c_1 can be considered negligible. Hence, the hypothesis of using a linear model in (1) is deemed acceptable.

The hydraulic suspension actuator, installed in the strut assembly, is modeled as a first order transfer function

$$\frac{u_a(s)}{u(s)} = \frac{1}{s\tau + 1} \quad (2)$$

where u is the actuator force demand, i.e., the system control input, and τ is the time constant of the transfer function.

The previous equations can be re-written into a continuous time state-space formulation

$$\begin{aligned} \dot{x}_{QC}(t) &= A_{QC}x_{QC}(t) + B_{QC}u(t) + E_{QC}w_0(t) \\ y_{QC}(t) &= C_{QC}x_{QC}(t) + D_{QC}u(t) \end{aligned} \quad (3)$$

where x_{QC} and y_{QC} are the state and output vectors; A_{QC} , B_{QC} , C_{QC} , and D_{QC} are the system matrices; E_{QC} is the road disturbance matrix; and t is time. $y_{QC}(t)$ contains the acceleration of the sprung mass \ddot{x}_1 .

The e-MPC uses a state feedback law. Hence, its performance depends on the accuracy and appropriate selection of the measured or estimated states. In the specific implementation, $x_{QC}(t) = [x_1 \ \dot{x}_1 \ x_1 - x_2 \ \dot{x}_1 - \dot{x}_2 \ u_a]^T$, i.e., x_{QC} contains the position and speed of the sprung mass, the suspension displacement and deflection rate, and the actual actuator force.

In the controller implementation, the estimates of x_1 and \dot{x}_1 are computed by high-pass filtering and integrating the vertical acceleration measurements of the vehicle body, through an algorithm already implemented on production vehicles with the same active suspension system of this article. $x_1 - x_2$ is obtained from the direct measurement of the active suspension actuator displacement and consideration of the suspension installation ratio, i.e., the ratio between the actuator displacement and the relative vertical displacement between the sprung and unsprung masses [42]. $\dot{x}_1 - \dot{x}_2$ is calculated through

differentiation of $x_1 - x_2$ with the hybrid smooth derivative method [43]. u_a is estimated from the measurements of the compression and rebound chamber pressures.

For preview control, the vertical road profile is modeled through a shift register, which is represented in discrete time form as

$$\begin{bmatrix} w_0(k+1) \\ w_1(k+1) \\ w_2(k+1) \\ \vdots \\ w_{N-1}(k+1) \\ w_N(k+1) \end{bmatrix} = \begin{bmatrix} 0 & 1 & 0 & 0 & \dots & 0 \\ 0 & 0 & 1 & 0 & \dots & 0 \\ 0 & 0 & 0 & 1 & \dots & 0 \\ \vdots & \vdots & \vdots & \vdots & \ddots & \vdots \\ 0 & 0 & 0 & 0 & \dots & 1 \\ 0 & 0 & 0 & 0 & \dots & 0 \end{bmatrix} \begin{bmatrix} w_0(k) \\ w_1(k) \\ w_2(k) \\ \vdots \\ w_{N-1}(k) \\ w_N(k) \end{bmatrix} + \begin{bmatrix} 0 \\ 0 \\ 0 \\ \vdots \\ 0 \\ 1 \end{bmatrix} y_r(k) \quad (4)$$

where k indicates the current time step. With simplified notations (4) can be rewritten as

$$\hat{w}(k+1) = [0 \quad A_{r,d}] \hat{w}(k) + E_{r,d} y_r(k) \quad (5)$$

where $\hat{w} = [w_0 \dots w_N]^T$ is the vector of the road system states, i.e., the road profile heights ahead of the tire, which consists of N points (see Fig. 1) equally spaced according to the time step Δt of the internal model; $A_{r,d}$ is the shift model matrix; $y_r(k) = w_N(k+1)$ is the disturbance input provided by the preview sensor measurement; and $E_{r,d}$ is the road system disturbance matrix.

By augmenting the state vector to $x(t) = [x_1 \quad \dot{x}_1 \quad x_1 - x_2 \quad \dot{x}_1 - \dot{x}_2 \quad u_a \quad \hat{w}]^T$, applying zero-order-hold discretization of the QC model (3) to obtain the system matrices $A_{QC,d}$, $B_{QC,d}$, $C_{QC,d}$, $D_{QC,d}$, and $E_{QC,d}$, and integrating the QC model with the road model (5), the complete vehicle-actuator-road system, indicated by the subscripts s in the remainder, reads

$$\begin{aligned} x(k+1) &= \begin{bmatrix} A_{QC,d} & E_{QC,d} & 0 \\ 0 & 0 & A_{r,d} \end{bmatrix} x(k) + B_{QC,d} u(k) \\ &+ \begin{bmatrix} 0 \\ E_{r,d} \end{bmatrix} y_r(k) \\ y(k) &= [C_{QC,d} \quad 0] x(k) + D_{QC,d} u(k) \end{aligned} \quad (6)$$

which can be simplified into

$$\begin{aligned} x(k+1) &= A_{s,d} x(k) + B_{QC,d} u(k) \\ &+ E_{s,d} y_r(k) \\ y(k) &= C_{s,d} x(k) + D_{QC,d} u(k). \end{aligned} \quad (7)$$

III. CONTROLLER FORMULATION

A. System Prediction

Given the initial state, $x(k)$, and the system in (7), the predicted output, \hat{y} , is calculated as

$$\begin{aligned} \hat{y} &= \begin{bmatrix} C_{s,d} A_{s,d} \\ C_{s,d} A_{s,d}^2 \\ \vdots \\ C_{s,d} A_{s,d}^p \end{bmatrix}_{p \times 1} x(k) \\ &+ \begin{bmatrix} C_{s,d} B_{QC,d} & \dots & 0 & 0 \\ \vdots & \ddots & \vdots & \vdots \\ C_{s,d} A_{s,d}^{p-1} B_{QC,d} & \dots & C_{s,d} B_{QC,d} & D_{QC,d} \end{bmatrix}_{p \times (c+1)} \hat{u} \end{aligned} \quad (8)$$

with

$$\hat{y} = \begin{bmatrix} y(k+1) \\ \vdots \\ y(k+p) \end{bmatrix}, \quad \hat{u} = \begin{bmatrix} u(k) \\ \vdots \\ u(k+c) \end{bmatrix} \quad (9)$$

where p and c are the number of steps corresponding to the prediction and control horizons, and \hat{u} is the control input over c , i.e., the vector of optimization variables. (8) can be shortened to

$$\hat{y} = \Lambda x(k) + \Theta_u \hat{u}. \quad (10)$$

The state predictions, \hat{x} , are computed with a similar method

$$\hat{x} = \Psi x(k) + \Omega_u \hat{u} \quad (11)$$

with

$$\hat{x} = \begin{bmatrix} x(k+1) \\ \vdots \\ x(k+p) \end{bmatrix} \quad (12)$$

where Λ , Θ_u , Ψ , and Ω_u are the resulting matrices.

B. Constrained Optimization and mp-QP Problem Formulation

A generic model predictive controller finds the optimal sequence of control inputs, \hat{u} , that minimizes a cost function, J_{MPC} , which depends on \hat{y} , \hat{x} , and \hat{u}

$$\begin{aligned} \min_{\hat{u}} J_{MPC} &= \min_{\hat{u}} (\hat{y}^T Q_1 \hat{y} + \hat{x}^T Q_2 \hat{x} + \hat{u}^T R \hat{u}) \\ \text{s.t. } &(x(k+i), u(k+i)) \in \mathcal{F}, \quad i = 0, \dots, p \end{aligned} \quad (13)$$

where Q_1 , Q_2 , and R are weight matrices, \mathcal{F} is a full-dimensional polyhedral set of appropriate dimensions, i is an integer, and p is the number of prediction steps, which defines the prediction horizon.

By substituting the formulations of the output and state predictions (respectively (10) and (11)) into (13), eliminating the terms not depending on \hat{u} , and dividing by 2, the optimization

problem becomes

$$\begin{aligned} \min_{\hat{u}} & \left(\frac{1}{2} \hat{u}^T (\Theta_u^T Q_1 \Theta_u + \Omega_u^T Q_2 \Omega_u + R) \hat{u} \right. \\ & \left. + x(k)^T (\Lambda^T Q_1 \Theta_u + \Psi^T Q_2 \Omega_u) \hat{u} \right) \\ \text{s.t. } & P \hat{u} \leq M_1 + M_2 x(k). \end{aligned} \quad (14)$$

The typical quadratic programming (QP) format is obtained through the simplification of (14)

$$\begin{aligned} \min_{\hat{u}} & \left(\frac{1}{2} \hat{u}^T H \hat{u} + x(k)^T F \hat{u} \right) \\ \text{s.t. } & P \hat{u} \leq M_1 + M_2 x(k) \end{aligned} \quad (15)$$

where H , F , P , M_1 , and M_2 are constant matrices. The initial states of the system are included in $x(k)$, the parameter vector.

A conventional i-MPC would execute an online optimization at each time step for a given value of $x(k)$, which is replaced by x in the remainder for the sake of brevity, and the control law would be implicitly obtained by the QP solver. In the e-MPC case, the optimization is performed offline, i.e., the QP problem is solved for the whole range of x , which explicitly generates $u = u(x)$. The optimization problem becomes a multiparametric QP (mp-QP) problem, generally described as the minimization of the objective function with the constraints defined in (15).

C. Objective Function

The key objective for ride comfort enhancement is the minimization of the vertical acceleration of the sprung mass. Additionally, the optimal solution has to consider the limitation of actuator displacement, chassis motion and wheel hop [44]. Hence, this article uses a cost function penalizing \ddot{x}_1 , $x_1 - x_2$, x_1 , and $x_2 - w_0$. The control effort u is also included to limit the actuation power consumption. The discrete form of the performance index to be minimized J_{MPC} is

$$\begin{aligned} J_{MPC} = & \sum_{i=1}^p \left(\rho_1 \ddot{x}_1(k+i)^2 + \rho_2 (x_1(k+i) - x_2(k+i))^2 \right. \\ & + \rho_3 x_1(k+i)^2 + \rho_4 (x_2(k+i) \\ & \left. - w_0(k+i))^2 \right) + \sum_{i=0}^c \rho_5 u(k+i)^2 \end{aligned} \quad (16)$$

where the factors ρ_i are the objective function weights, which define Q_1 , Q_2 , and R in (13). In the specific implementation, the constraints are related to the actuator force and suspension displacement.

D. Decentralized Controller

To reduce the e-MPC generation time, memory requirements and implementation complexity, a decentralized control architecture is adopted, with one independent e-MPC at each vehicle corner. In fact, each QC-actuator-road model inherits only

$5 + (N + 1)$ mp-QP parameters. In contrast, a centralized suspension controller would have to be based on a seven-degree-of-freedom (7-DOF) model to consider the vertical dynamics of the unsprung masses, the heave, pitch, and roll dynamics of the sprung mass, the actuator dynamics, and the road model for each corner. This would result in a considerably larger problem, with $18 + 4(N + 1)$ mp-QP parameters.

E. Regionless e-MPC

In the e-MPC implementation, the solution of the mp-QP problem in (15) is computed offline. The solution is the function $\hat{u}^*(x)$, which is piecewise affine and maps the parameter vector onto the sequence of optimal control inputs. The e-MPC uses only the control input at the first time step, i.e., $u(x) = [I \ 0 \ \dots \ 0] \hat{u}^*(x)$, and the online implementation reduces to a simple function evaluation.

In the region-based e-MPC [33], the explicit representation of the control action is a piecewise affine state feedback law, defined by a partitioning of the state-space into m polyhedral critical regions

$$u(x) = \begin{cases} L_1 x + l_1, & S_1 x \leq s_1 \\ \vdots & \vdots \\ L_m x + l_m, & S_m x \leq s_m \end{cases} \quad (17)$$

where L_i , l_i , S_i , and s_i are constant matrices that are stored in the control hardware. The benefit of this method is the reduction of the online computational requirements with respect to the more common i-MPC. On the downside, the method yields increased memory requirements, especially for systems with a large number of parameters, and significant offline calculations. The first point is a major issue of the region-based method applied to preview suspension control, in particular, if multiple preview points (i.e., e-MPC parameters) are included in the model in (4).

To mitigate the weaknesses of the region-based e-MPC, this article adopts the recently proposed regionless e-MPC approach, described in [34] and [35]. The method does not need to compute or store the critical regions, defined by S_i and s_i . In fact, in the offline process all the possible active sets $\{A_1, \dots, A_{N_R}\}$ that can be locally optimal are considered through the extensive enumeration method in [45], where N_R is the number of regions. A linear program based on the Karush–Kuhn–Tucker conditions is solved to determine the feasibility of the candidate active sets. For each locally optimal active set the solution is

$$\hat{u}^* = -H^{-1} (F^T x + P_{A_i}^T \lambda^*) \quad (18)$$

where P_{A_i} includes only the rows of P indexed by the set of active constraints, and λ^* represents the dual variables given by

$$\lambda^* = Q(A_i) x + q(A_i) \quad (19)$$

with

$$Q(A_i) = -(P_{A_i} H^{-1} P_{A_i}^T)^{-1} (M_{2A_i} + P_{A_i} H^{-1} F^T) \quad (20)$$

$$q(A_i) = -(P_{A_i} H^{-1} P_{A_i}^T)^{-1} M_{1A_i} \quad (21)$$



Fig. 2. ACOCAR vehicle demonstrator with preview sensor.

where M_{1A_i} and M_{2A_i} contain only the rows of M_1 and M_2 corresponding to the active set A_i . The maps of $Q(A_i)$ and $q(A_i)$ are generated offline and stored in the controller together with H^{-1} , F , P , M_1 , and M_2 .

In the online implementation of the regionless controller, (18)–(19) are used to calculate \hat{u}^* , by finding the optimal active set for the current x from the list of locally optimal active sets. In particular, the optimal active set must fulfil the conditions

$$\begin{aligned} \lambda^* &\geq 0 \\ P\hat{u}^* &< M_1 + M_2x. \end{aligned} \quad (22)$$

The details of the online algorithm are reported in [45]. The resulting control action is identical to the one generated by the region-based e-MPC, i.e., the regionless and region-based implementations bring exactly the same results.

IV. CONTROL SYSTEM IMPLEMENTATION

A. Vehicle Demonstrator

The decentralized controller was implemented on a sport utility vehicle (SUV) demonstrator (see Fig. 2) with a hydraulic active suspension system—the Tenneco Monroe intelligent suspension, ACOCAR. At each vehicle corner, a pump pressurizes the hydraulic circuit of the actuator and thereby inputs energy into the system. The pressure level in the hydraulic chamber is modulated through the currents of the base and piston valves of the actuator, which is installed in parallel to an air spring. This actuation system mainly targets roll, pitch and primary ride control (see [46], [47] for the definition of primary ride), i.e., it is designed for input frequencies <4 Hz, but usually causes degradation of the secondary ride comfort performance, i.e., for frequencies >4 Hz. The vehicle demonstrator has a double wishbone suspension on the front axle, and a multilink suspension system on the rear axle, with installation ratios of 0.7 and 0.76.

The relevant sensor set consists of the following:

- 1) three vertical acceleration sensors installed on the sprung mass, two of them located in proximity of the front bumper, and one in proximity of the rear bumper;
- 2) a three-degree-of-freedom (3-DOF) inertial measurement unit;
- 3) suspension displacement sensors;
- 4) a preview sensor, i.e., the solid state LiDAR XenoTrack, mounted on the roof of the car.

A three-dimensional (3-D) model of the road ahead is constructed (i.e., a rolling carpet), and only the road profile heights directly in front of the wheels are sent to the e-MPCs. The accuracy and robustness of the preview road profile signal was guaranteed via appropriate high-pass filtering of the sensor outputs, a compensation algorithm of the sprung mass motion, and experimental tests to obtain the synchronization lag values.

All controllers and state estimators were installed on the dSPACE MicroAutoBox II system of the vehicle, which has a 16 MB flash memory. The regionless e-MPCs were integrated into the ACOCAR suspension control software framework to interface with the hardware. A low-level actuator management system calculates the reference currents for the compression and rebound valves, as well as the pump reference speed, as functions of u and $\dot{x}_1 - \dot{x}_2$. The current driver modules of the production suspension system feed the actuator valves and pumps.

B. Model Validation

Measurements of the ACOCAR vehicle demonstrator response on a four-poster test rig were used for the validation of two simulation models: a) a 7-DOF model for control system assessment, implemented in MATLAB/Simulink. This model considers heave, roll and pitch of the sprung mass, and vertical displacement of each unsprung mass, and includes a simplified model of the actuation system dynamics; and b) the internal e-MPC model, i.e., the QC model described in Section II.

The four-poster test rig was set up to emulate a typical ISO C–D ride comfort assessment road [48]. During the experiments, a fixed current of 0.4 A was applied to the piston and base valves of the actuators to maximize the size of the valve orifices, and, thus, achieve minimum damping.

The reported experimental values were calculated from the vertical acceleration and actuator displacement measurements, by using the state estimator of the ACOCAR suspension system. The time domain results were converted into the frequency domain, and are shown in Fig. 3 in terms of power spectral densities (PSDs). A good match between the 7-DOF model and the real vehicle is observed up to ~ 15 Hz, which is in line with the model bandwidth. In particular, the 7-DOF model captures the resonance peak of the sprung mass at ~ 1 – 1.5 Hz, and those of the unsprung masses at ~ 10 – 12 Hz.

The e-MPC internal model in (1) was validated in a similar way, i.e., the front and the rear QC model outputs were compared with the experimental displacements of the suspension top mounts and wheels. A good level of modeling accuracy was achieved also in this case, as shown in Fig. 4.

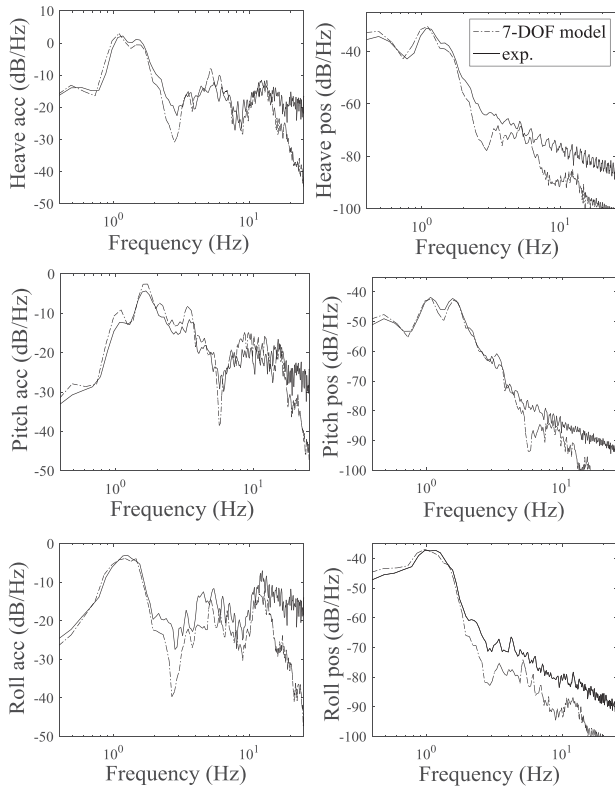


Fig. 3. Example of experimental validation of the 7-DOF model along the ride comfort road profile emulated on the four-poster test rig: PSDs of sprung mass accelerations and positions.

The e-MPC internal actuator model in (2) was validated with actuator test rig data. For example, Fig. 5 shows the time histories of the force demand, measured force and simulated force for step-in and step-out force demand tests. A good match was achieved with $\tau = 50$ ms, despite the simplicity of the model formulation.

C. Explicit Controller Generation and Implementation

According to the internal model formulation in (7), discretized at $\Delta t = 10$ ms, each controller is based on 8 mp-QP parameters, i.e., the four states of the QC model, one state for the actuator, and three states ($N = 2$) for the road profile ahead according to (4).

Simulations on a ride comfort road and a speed bump were carried out to evaluate the independent and combined effects of p , i.e., the prediction horizon, c , i.e., the control horizon, and N , i.e., the number of preview points. It was verified that in the specific test scenarios the increase of p and c brings significant benefits. Therefore, p and c were assigned relatively large values, respectively, 8 and 6. On the contrary, N was tuned to be as low as possible, to reduce the required flash memory size (which strongly varies with N) without significantly affecting comfort. At 50 km/h, the selected parametrization corresponds to a ~ 0.3 m look ahead distance and a > 1 m prediction distance.

An inequality constraint was applied to the actuator force magnitude, i.e., < 9000 N. The tuning of the cost function

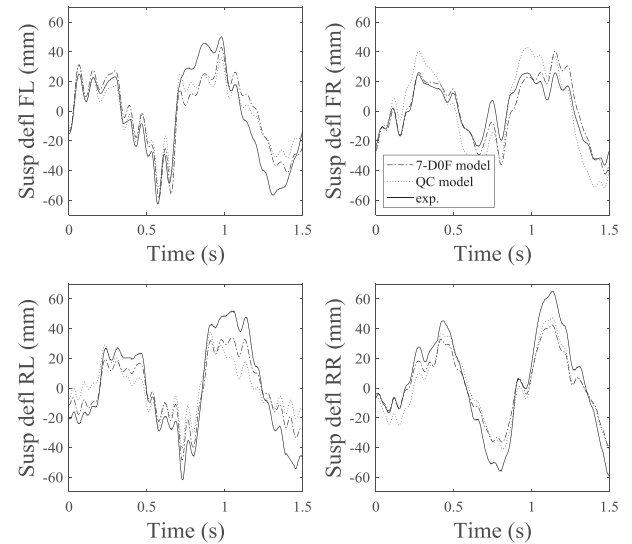


Fig. 4. Example of experimental validation of the 7-DOF and QC models along the ride comfort road profile emulated on the four-poster test rig: time histories of suspension deflections. The subscripts FL, FR, RL, and RR indicate the front left, front right, rear left, and rear right corners.

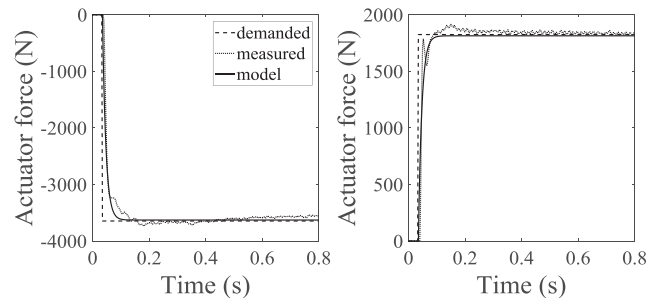


Fig. 5. Example of experimental validation of the e-MPC internal actuator model for step-in and step-out force demand tests.

(16) prioritized the reduction of the vertical acceleration and displacement of the sprung mass, by choosing greater values for ρ_1 and ρ_3 relative to ρ_2 and ρ_5 . ρ_4 was only used for a preliminary feasibility check in simulation, targeting the wheel hop reduction, while it was set to 0 in the experiments as wheel hop was not observed.

The mp-QP problems for the active suspension system with and without preview were solved with a custom version of the multiparametric toolbox 3 [49] that included the regionless solver RLENUMPQP. The solution was considered over a bounded partition of the state-space, with the following limits: ± 0.1 m in body displacement; ± 0.5 m/s in body velocity; ± 0.15 m in suspension displacement; ± 4 m/s in suspension velocity; and ± 0.15 m in road displacement.

Table II gives the comparison of the region-based and regionless algorithms, in terms of solution generation time and corresponding memory requirements, where the reduction of the latter is of the essence for the industrial implementation of the algorithm. In particular, the industrial partners of this article specified an upper limit of 1 MB memory to ensure applicability to a production-ready suspension system. As indicated by

TABLE II

EXPLICIT SOLUTION GENERATION TIME AND MEMORY DEMAND OF THE REGION-BASED AND REGIONLESS E-MPC APPROACHES

Method	Generation time	Memory demand
Region-based, w/o preview	3 s	~600 kB
Regionless, w/o preview	3 s	~30 kB
Region-based, w/ preview	140 s	~30 MB
Regionless, w/ preview	21 s	~1 MB

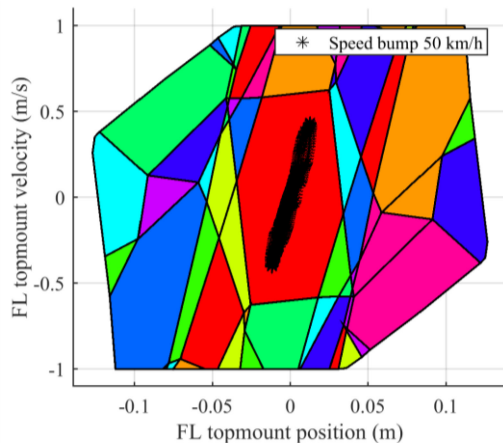
Fig. 6. Critical regions on the $\dot{x}_1(x_1)$ plane for the e-MPC with preview tested on the vehicle demonstrator.

Table II, the regionless e-MPC achieves this specification for both configurations, with and without preview, which is an important outcome of this article. To meet the 1 MB memory specification at the vehicle level for the system with preview, and verify the system robustness with respect to the modeling uncertainty, the same regionless explicit solution was implemented on the front and rear suspensions, despite a marginal difference in their parameters. In contrast, the traditional region-based e-MPC solution obtained with the ENUMQP solver meets the memory specification only for the nonpreview version, and significantly exceeds the limit when preview is included. Moreover, the online algorithm of the regionless e-MPC required, on average, only 0.09 ms run time (with a maximum of 0.2 ms) on the dSpace platform during a typical test. The short computation times therefore allow the implementation of the controller at almost any time-step used in automotive applications.

With the regionless approach, the regions do not need to be calculated, but they can be reconstructed and visualized *a posteriori*. For the specific preview controller, the solution is a set of affine functions over 1099 polyhedral regions. Figs. 6 and 7 show two-dimensional (2-D) slices over the multidimensional state-space. Such representation of the explicit control law allows the formal analysis of the stability and robustness properties of the resulting controller. The figures also report the operating points of the system along a speed bump at 50 km/h. The analysis of the actual operating points of the vehicle in real maneuvers is useful to understand whether specific portions of the e-MPC control law can be adopted to formulate a simplified rule-based controller.

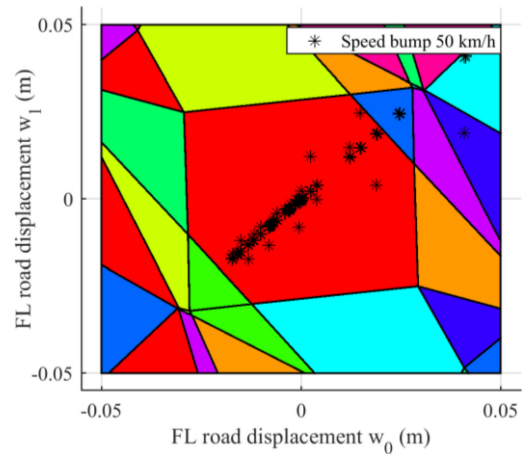
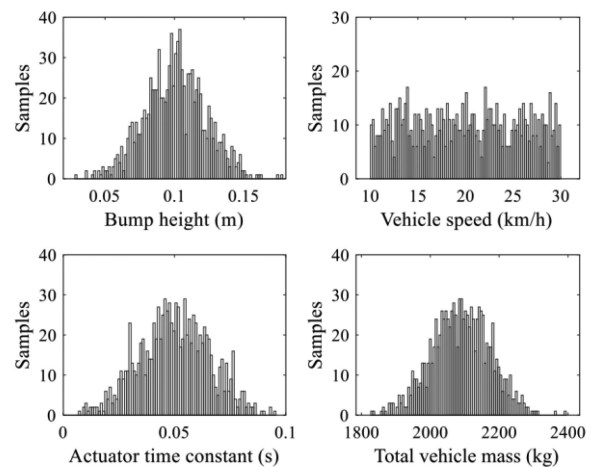
Fig. 7. Critical regions on the $w_1(w_0)$ plane, for the e-MPC with preview tested on the vehicle demonstrator.

Fig. 8. Distribution of the randomly selected parameters of the Monte Carlo analysis.

D. e-MPC Stability

From a theoretical viewpoint, the closed-loop stability of the proposed e-MPC can be achieved by including the term $x^T(k+p)Zx(k+p)$ into the objective function (16) via (15), where Z is the solution of the algebraic Riccati equation for the system in (7), along with the constraint $x(k+p) \in \Theta$, where Θ is a positive invariant set for the system. However, stability can also be achieved by appropriately choosing the state and input weighting coefficients ρ_i in (16). Typically, selecting the state weights significantly larger than the input weight ρ_5 helps to achieve a stable behavior of the closed-loop system, which is the tuning method used here.

In this article, the stability of the controller was verified through Monte Carlo simulations. The e-MPC strategy was tested in 1000 challenging scenarios, each set up with a different vehicle mass, speed and actuator response time. The simulations were performed over a 1-m long speed bump with a height that was also changed between runs. Fig. 8 shows the distribution of the randomly selected values of the four parameters. The

controller was considered stable if the suspension deflections at each corner of the 7-DOF model did not exceed 5 mm, 3 s after the front axle hit the bump. Stability was achieved in all cases.

E. Benchmark Controller: Centralized Skyhook

A centralized skyhook algorithm [51], already implemented and tested on the case study vehicle demonstrator, was used as the experimental benchmark for the decentralized e-MPCs. In the skyhook approach, the total sprung mass reference heave force F_h , antipitch moment M_p , and antiroll moment M_r , are calculated as

$$\begin{bmatrix} F_h \\ M_p \\ M_r \end{bmatrix} = \begin{bmatrix} c_h & 0 & 0 \\ 0 & c_p & 0 \\ 0 & 0 & c_r \end{bmatrix} \begin{bmatrix} \dot{x}_{s,est} \\ \dot{\theta}_{est} \\ \dot{\varphi}_{est} \end{bmatrix} \quad (23)$$

where c_h , c_p , and c_r are the skyhook damping coefficients for the heave, pitch and roll motions; and $\dot{x}_{s,est}$, $\dot{\theta}_{est}$, and $\dot{\varphi}_{est}$ are the estimated heave, pitch and roll rates of the sprung mass. The matrix form of (23) is $F_{sh} = c_{sh} V_{est}$, where F_{sh} is the vector of the total skyhook force and moments, c_{sh} is the matrix of the skyhook coefficients, and V_{est} is the vector including the three speeds in (23). In addition, $F_{sh} = L u_{c,sh}$, where $u_{c,sh}$ is the vector of the skyhook actuation forces at the four corners, i.e., the outputs of the controller, and L is the matrix with the coefficients to calculate the resulting force and moments acting on the sprung mass. The terms of L include the geometric vehicle parameters, e.g., the front and rear semi-wheelbases h_F and h_R ; and track widths t_F and t_R . In the controller implementation, a pseudoinverse formulation is used to obtain the control action vector $u_{c,sh}$

$$u_{c,sh} = [u_{FL} \quad u_{FR} \quad u_{RL} \quad u_{RR}]^T = (L^T L)^{-1} L^T c_{sh} V_{est} \quad (24)$$

with

$$L = \begin{bmatrix} -1 & -1 & -1 & -1 \\ h_F & h_F & -h_R & -h_R \\ \frac{t_F}{2} & -\frac{t_F}{2} & \frac{t_R}{2} & -\frac{t_R}{2} \end{bmatrix} \quad (25)$$

where the notations FL , FR , RL , and RR indicate the front left, front right, rear left, and rear right corners.

V. RESULTS

A. Simulation Results

The 7-DOF vehicle model was used for the virtual validation of the controllers along a ride comfort track, at a constant speed of 60 km/h. The analysis involved the regionless e-MPC implementations, including and excluding preview, and their performance comparison with the passive vehicle, i.e., the case study SUV without active suspensions. The simulations with the controllers were based on realistic data of next-generation suspension actuators with higher bandwidth than those installed on the real vehicle demonstrator, and under the hypothesis of perfect synchronization of the preview input with the actual road profile at the wheels. This set-up was chosen to assess

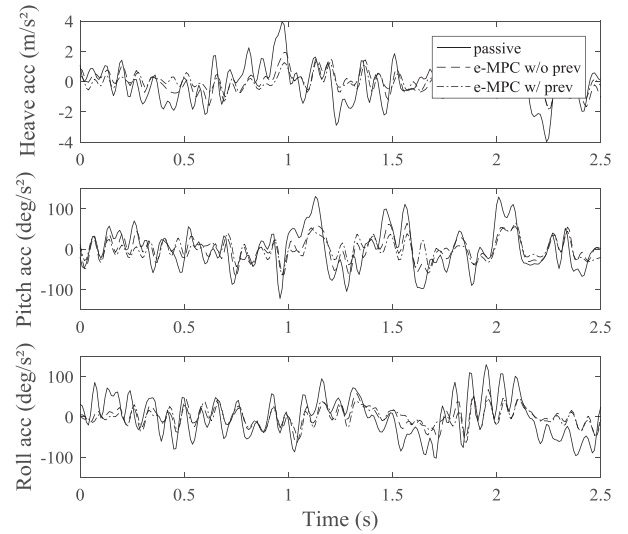


Fig. 9. Time domain plots of heave, pitch and roll accelerations obtained on a simulated section of the ride comfort road at 60 km/h.

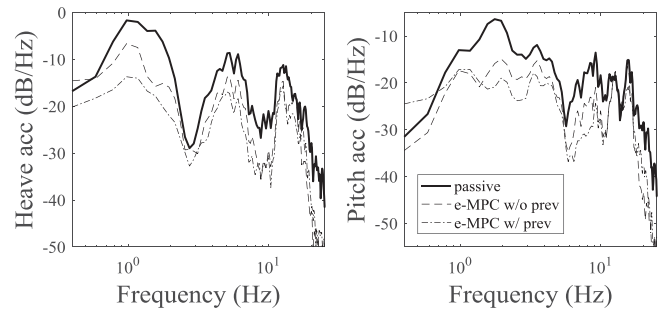


Fig. 10. Simulation of a ride comfort road at 60 km/h: PSDs of the heave and pitch accelerations.

TABLE III
RMS VALUES OF THE SPRUNG MASS ACCELERATIONS FOR THE SIMULATED RIDE COMFORT ROAD AT 60 KM/H

	Mode	Pass.	e-MPC w/o preview	e-MPC w/ preview
Non freq. weighted	Heave (m/s ²)	1.00	0.53 (-47%)	0.34 (-35%)
	Pitch (rad/s ²)	0.63	0.34 (-47%)	0.27 (-19%)
	Roll (rad/s ²)	0.63	0.32 (-48%)	0.26 (-21%)
Freq. weighted	Heave (m/s ²)	0.73	0.39 (-46%)	0.28 (-29%)
	Pitch (rad/s ²)	0.29	0.13 (-55%)	0.11 (-13%)
	Roll (rad/s ²)	0.34	0.17 (-51%)	0.12 (-27%)

Note: The % variations are with respect to the system in the column to the immediate left.

the medium-to-long-term potential of the e-MPC preview technology.

Fig. 9 reports the time histories of the heave, pitch, and roll accelerations for a section of the run. In particular, the passive set-up has a 3.96 m/s² peak heave acceleration, which is reduced to 1.91 and 1.26 m/s² for the e-MPCs without and with preview. Fig. 10 shows the results in terms of PSD profiles of the heave and pitch accelerations, while Table III reports the

root-mean-square (RMS) values of the vehicle body accelerations $a_{i,\text{RMS}}$ for heave, pitch and roll, calculated as

$$a_{i,\text{RMS}} = \left(\int_{f_1}^{f_2} \text{PSD}_i(f) df \right)^{0.5} \quad (26)$$

where f is the frequency, and f_1 and f_2 are the boundaries of the considered frequency range. In the PSD plots, the benefits of the controllers are evident for the 0–15 Hz range. This confirms the appropriateness of the e-MPC designs for improving both primary ride and secondary ride. In particular, the e-MPC without preview reduces the $a_{i,\text{RMS}}$ values by more than 45% with respect to the passive vehicle, while the introduction of preview brings a further improvement, ranging from 19 to 35% depending on the considered acceleration.

The table also includes the RMS values of the heave, pitch and roll accelerations of the vehicle sprung mass, after the application of frequency weighting functions according to [52]. In particular, the heave acceleration is weighted more in the 4–8 Hz frequency band than in the other frequency ranges. The overall improvements brought by the e-MPCs are similar to those without frequency weighting and consistent with the results in Table I, which confirms the all-around effectiveness of the proposed controllers.

As the actuation dynamics represent an unmatched uncertainty in the system, ride comfort road simulations at 60 km/h were run to assess robustness with respect to the actuator time constant τ , which was varied up to 300 ms (six times the value for the available hydraulic actuators), while keeping the e-MPC tuned for the nominal τ . The results show that the controllers without and with preview perform significantly better than the passive set-up, and the active setup with preview always provides the best performance.

B. Experimental Results

The performance of the e-MPCs (excluding and including preview) was experimentally tested with the ACOCAR vehicle demonstrator (see Section IV-A) and compared to the car with the active skyhook controller (Section IV-E) and a passive suspension set-up. The passive set-up was obtained by applying fixed currents to the actuator valves to achieve a suspension tuning that is close to the one of the passive version of the SUV.

The experiments consisted of two tests carried out on the public roads of Sint Truiden (Belgium).

- 1) *Test 1*: Driving over a short wavelength speed bump with a height of 5 cm and a length of 0.4 m, at approximately 30 km/h.
- 2) *Test 2*: Driving over a long wavelength speed bump with a height of 15 cm and a length of 2.5 m, at approximately 50 km/h, which causes significantly higher accelerations than test 1.

The tests were repeated several times to verify the reliability of the measurements. Fig. 11 shows the time history of the heave position and pitch angle of the vehicle body for test 2. The results confirm the reduction of the sprung mass motion when negotiating the bump. For instance, the passive and skyhook

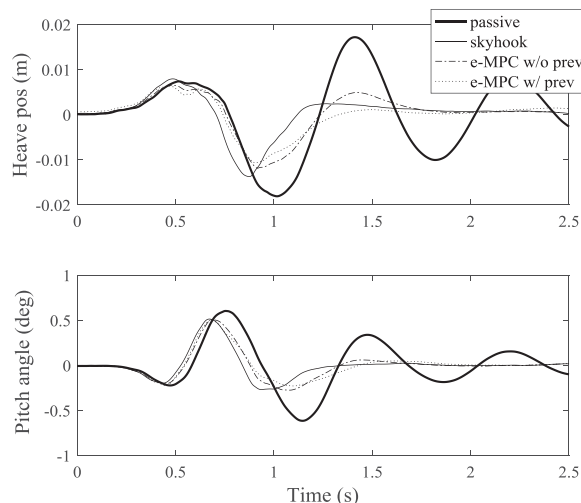


Fig. 11. Experimental results for test 2: Time domain plots of the heave position and pitch angle.

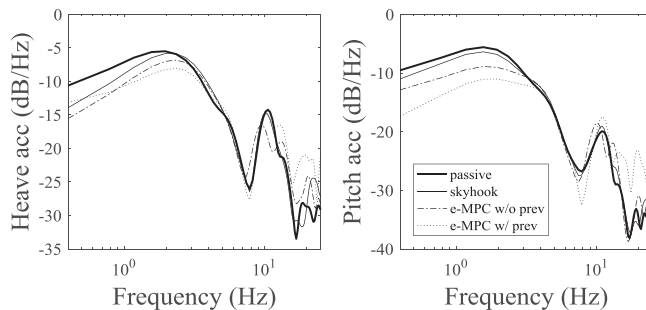


Fig. 12. Experimental results for test 1: PSDs of the heave and pitch accelerations.

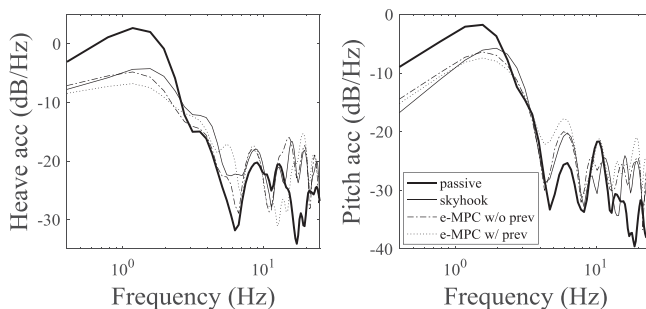


Fig. 13. Experimental results for test 2: PSDs of the heave and pitch accelerations.

set-ups have heave displacements of -0.018 and -0.014 m at the first negative oscillation peak. For the e-MPCs without and with preview, these values are reduced to -0.011 and -0.010 m.

Figs. 12 and 13 show the PSD results in the frequency domain. Tables IV and V report the RMS values of the heave and pitch accelerations of the vehicle sprung mass without and with frequency weighting, up to 15 Hz, i.e., well beyond the

TABLE IV
RMS VALUES OF THE SPRUNG MASS ACCELERATIONS DURING TEST 1

	Mode	Freq. range	Pass.	Skyhook	e-MPC w/o preview	e-MPC w/ preview
Non freq. weighted	Heave (m/s ²)	0-4 Hz	0.86	0.82 (-4%)	0.74 (-11%)	0.66 (-10%)
		0-15 Hz	0.95	0.92 (-3%)	0.83 (-9%)	0.80 (-4%)
	Pitch (rad/s ²)	0-4 Hz	0.81	0.75 (-8%)	0.61 (-17%)	0.49 (-21%)
0-15 Hz		0.85	0.80 (-7%)	0.68 (-14%)	0.57 (-16%)	
	a_p (m/s ²)	0-15 Hz	0.51	0.48 (-6%)	0.43 (-10%)	0.39 (-9%)
Freq. weighted	Heave (m/s ²)	0-15 Hz	0.67	0.65 (-3%)	0.62 (-5%)	0.63 (+2%)
	Pitch (rad/s ²)	0-15 Hz	0.51	0.50 (-1%)	0.36 (-27%)	0.29 (-21%)
	a_p (m/s ²)	0-15 Hz	0.34	0.33 (-3%)	0.29 (-12%)	0.27 (-7%)

Note: The % variations are with respect to the system in the column to the immediate left.

TABLE V
RMS VALUES OF THE SPRUNG MASS ACCELERATIONS DURING TEST 2

	Mode	Freq. range	Pass.	Skyhook	e-MPC w/o preview	e-MPC w/ preview
Non freq. weighted	Heave (m/s ²)	0-4 Hz	1.60	0.87 (-45%)	0.78 (-11%)	0.69 (-12%)
		0-15 Hz	1.61	0.93 (-42%)	0.84 (-9%)	0.74 (-12%)
	Pitch (rad/s ²)	0-4 Hz	0.99	0.68 (-31%)	0.63 (-7%)	0.58 (-8%)
0-15 Hz		1.00	0.70 (-30%)	0.66 (-6%)	0.63 (-4%)	
	a_p (m/s ²)	0-15 Hz	0.76	0.47 (-38%)	0.43 (-9%)	0.38 (-12%)
Freq. weighted	Heave (m/s ²)	0-15 Hz	0.82	0.55 (-32%)	0.50 (-10%)	0.47 (-5%)
	Pitch (rad/s ²)	0-15 Hz	0.70	0.39 (-43%)	0.41 (+4%)	0.37 (-8%)
	a_p (m/s ²)	0-15 Hz	0.43	0.27 (-37%)	0.26 (-4%)	0.24 (-8%)

Note: The % variations are with respect to the system in the column to the immediate left.

bandwidth of the specific actuators. The roll acceleration results are omitted, as roll motion was not excited by these tests.

As expected, given the relatively low bandwidth of the specific actuators, the controlled set-ups mainly improve primary ride, i.e., the range of 0–4 Hz. For example, in this frequency range, the e-MPC without preview improves the RMS heave acceleration performance without frequency weighting in both tests by 11% compared to the skyhook. The addition of preview reduces the RMS accelerations by a further 10% and 12% in tests 1 and 2. The e-MPC without preview reduces the pitch accelerations by 17% and 7% in the two tests compared to the skyhook, while the preview adds a further benefit, i.e., 21% in test 1 and 8% in test 2.

The results are confirmed over the 0–15 Hz frequency band. For instance, the RMS values of the heave acceleration in the two tests are 0.95 and 1.61 m/s² for the passive set-up, while the e-MPC with preview reduces the values to 0.80 and 0.74 m/s². In the same frequency range, the heave acceleration performance of the e-MPC with preview is consistently better than that of the e-MPC without preview; 4% improvement during test 1 and 12% improvement during test 2. Similarly, the preview reduces the RMS of the pitch motion by 16% and 4%. Moreover, the e-MPC without preview consistently outperforms the skyhook algorithm, e.g., by 9% in terms of heave acceleration. An important conclusion is that despite the decentralized architecture of the implemented e-MPCs, the associated vehicle performance improvement is evident also in terms of pitch acceleration. In fact, the RMS values of pitch acceleration with the skyhook

controller are 14% and 6% higher than with the e-MPC without preview. This result is particularly remarkable considering that the skyhook controller includes a term directly targeting the pitch dynamics. Also, the level of technology maturity of its implementation on the vehicle demonstrator is significantly higher than that of the proposed e-MPCs.

In general, the RMS values of the heave and pitch frequency weighted accelerations of the vehicle sprung mass in the 0–15 Hz frequency range tend to generate more limited controller benefits in comparison with the non-weighted results. This is mainly due to the actuator bandwidth, and the fact that the frequency weighting functions were not accounted for in the cost function (16) nor in the tuning of the e-MPC parameters, which is the subject of future work. Nevertheless, the e-MPCs still show considerable benefits over the skyhook.

As a summary of the performance benefit, **Tables IV and V** also include the vibration total value a_v i.e., an indicator that combines vibrations in multiple directions [52]

$$a_v = (k_h^2 a_{h,RMS}^2 + k_p^2 a_{p,RMS}^2)^{0.5} \quad (27)$$

where $a_{h,RMS}$ and $a_{p,RMS}$ are the RMS heave and pitch accelerations. k_h and k_p are the multiplying factors, both set to 0.4. In test 1, the skyhook reduces the a_v indicator based on the frequency weighted accelerations by only 3% with respect to the passive vehicle, while the e-MPCs without and with preview outperform the production skyhook controller by 12% and a further 7%. In test 2, despite the already excellent performance of the skyhook, which provides a 37% improvement over the passive case, the e-MPCs without and with preview further reduce the vibration total value by 4% and 8%. Such preliminary experimental benefits are aligned with the literature in **Table I**, which is mainly based on simulation results, and encourage the further industrial development of regionless e-MPC for active suspension control.

VI. CONCLUSION

To the best of our knowledge, for the first time this article implemented a regionless e-MPC strategy for an active suspension system with and without preview. The activity allows the following conclusions.

- 1) The internal QC models of the decentralized e-MPC architecture provide a sufficiently good match with the experimental data, and can be considered simple yet appropriate formulations for suspension control design.
- 2) The regionless e-MPC with preview based on a QC model brings a memory requirement reduction by a factor of ~ 30 , compared to the corresponding region-based e-MPC.
- 3) The e-MPC simulation results with hydraulic actuators along a ride comfort road show reductions of the RMS values of the sprung mass accelerations in excess of 45% relative to the passive car, and a further benefit (up to 35%) is achieved with the addition of preview.
- 4) The preliminary experimental results along two speed bump road inputs on a vehicle demonstrator with active suspension actuators show that, compared to the more

conventional skyhook, the e-MPC without preview improves primary ride performance—with reductions of primary ride vehicle body accelerations ranging from 7 to 17%. The addition of preview further reduces primary ride accelerations by 8 to 21%. All the evaluated e-MPC implementations improve the vibration total value in the 0–15 Hz frequency range, which indicates their overall ride comfort enhancement capability.

Future developments will include the systematic optimization of the tuning parameters of the proposed controllers, and the assessment of centralized control approaches based on regionless e-MPC technology.

REFERENCES

- [1] E.K. Bender, "Optimum linear preview control with application to vehicle suspension," *J. Basic Eng.*, vol. 90, no. 2, pp. 213–221, 1968.
- [2] Y. Iwata and M. Nakano, "Optimum preview control of vehicle air suspension," *Bull. Jpn. Soc. Mech. Eng.*, vol. 19, no. 138, pp. 1485–1489, 1976.
- [3] Y. Iwata and M. Nakano, "Optimal preview control of vehicle suspension," *Bull. Jpn. Soc. Mech. Eng.*, vol. 19, no. 129, pp. 265–273, 1976.
- [4] W. A. H. Oraby, M. A. Aly, S. M. El-Demerdash, and A. M. Selim, "Influence of active suspension preview control on the vehicle lateral dynamics," SAE Tech. Paper 2007-01-2347, 2007.
- [5] R. Streiter, "Active preview suspension system ABC prescan in the F700," *ATZ Worldwide*, vol. 110, pp. 4–11, 2008.
- [6] A. Schindler, "Neue Konzeption und erstmalige Realisierung eines aktiven Fahrwerks mit Preview-Strategie." Ph.D. thesis, Karlsruhe Inst. Technol., Karlsruhe, Germany, 2009.
- [7] M. Kaldas *et al.*, "Preview enhanced rule-optimized fuzzy logic damper controller," SAE Tech. Paper 2014-01-0868, 2014.
- [8] A. Desikan and V. Kalachelvi, "Design for a semi-active preview suspension system using fuzzy-logic control and image processing techniques," presented at the IEEE Int. Conf. Cyber Technol. Automat., Control Intell. Syst., 2015.
- [9] A. M. A. Soliman and D. A. Crolla, "Limited bandwidth active suspension employing wheel base preview," SAE Tech. Paper 2001-01-1063, 2001.
- [10] F. Jun-ping, Y. Shao-yi, and Z. Lan-chun, "Research on wheelbase preview control for vehicle semi-active suspension based on neural networks," presented at the IEEE Int. Symp. Intell. Inf. Technol. Appl., 2009.
- [11] M. Tomizuka, "Optimal preview control with application to vehicle suspension," *J. Dyn. Syst., Meas., Control*, vol. 98, no. 3, pp. 309–315, 1976.
- [12] A. Hac, "Optimal linear preview control of active vehicle suspension," in *Proc. IEEE Conf. Decis. Control*, 1990, pp. 2779–2784.
- [13] M. A. H. van der Aa, J. H. E. A. Muijderland, and F. E. Veldpaus, "Constrained optimal control of semi-active suspension systems with preview," *Veh. Syst. Dyn.*, vol. 28, no. 4/5, pp. 307–323, 1997.
- [14] D. Martinus, B. Soenarko, and Y. Y. Nazaruddin, "Optimal control design with preview for semi-active suspension on a half-vehicle model," in *Proc. IEEE Conf. Decis. Control*, 1996, pp. 2798–2803.
- [15] A. G. Thompson and C. E. M. Pearce, "Performance index for a preview active suspension applied to a quarter-car model," *Veh. Syst. Dyn.*, vol. 35, no. 1, pp. 55–66, 2001.
- [16] G. Prokop and R.S. Sharp, "Performance enhancement of limited bandwidth active automotive suspensions by road preview," *IEEE J. Control Theory Appl.*, vol. 142, no. 2, pp. 140–148, Mar. 1995.
- [17] H. J. Kim, H. S. Yang, and Y. P. Park, "Improving the vehicle performance with active suspension using road-sensing algorithm," *J. Comput. Struct.*, vol. 80, no. 18–19, pp. 1569–1577, 2002.
- [18] A. Akbari and B. Lohmann, "Output feedback H_∞/GH_2 preview control of active vehicle suspensions: A comparison study of LQG preview," *J. Veh. Syst. Dyn.*, vol. 48, no. 12, pp. 1475–1494, 2010.
- [19] R. S. Prabakar, C. Sujatha, and S. Narayanan, "Optimal semi-active preview control response of a half car vehicle model with magnetorheological damper," *J. Sound Vib.*, vol. 326, no. 3–5, pp. 400–420, 2009.
- [20] S. Ryu, Y. Park, and M. Suh, "Ride quality analysis of a tracked vehicle suspension with a preview control," *J. Terramechanics*, vol. 48, no. 6, pp. 409–417, 2011.
- [21] P. Li, J. Lam, and K. Chung Cheung, "Multi-objective control for active vehicle suspension with wheelbase preview," *J. Sound Vib.*, vol. 333, no. 21, pp. 5269–5282, 2014.
- [22] R. K. Mehra, J. N. Amin, K. J. Hedrick, C. Osorio, and S. Gopalasamy, "Active suspension using preview information and model predictive control," in *Proc. IEEE Int. Conf. Control Appl.*, 1997, pp. 860–865.
- [23] M. D. Donahue and J. K. Hedrick, "Implementation of an active suspension, preview controller for improved ride comfort," 2002.
- [24] M. Ahmed and F. Svaricek, "Preview optimal control of vehicle semi-active suspension based on partitioning of chassis acceleration and tire load spectra," in *Proc. IEEE Eur. Control Conf.*, 2014, pp. 1669–1674.
- [25] S. De Bruyne, H. Van der Auweraer, and J. Anthonis, "Preview control of a constrained hydraulic active suspension system," in *Proc. IEEE Conf. Decis. Control*, 2012, pp. 4400–4405.
- [26] S.M. Savaresi *et al.*, "Optimal Strategy for Semi-Active Suspensions and Benchmark," in *Semi-Active Suspension Control Design for Vehicles*, Amsterdam, The Netherlands: Elsevier, 2010, ch. 5.
- [27] C. Göhrle *et al.*, "Design and vehicle implementation of preview active suspension controllers," *IEEE Trans. Control Sys. Technol.*, vol. 22, no. 3, pp. 1135–1142, May 2014.
- [28] C. Göhrle *et al.*, "Road profile estimation and preview control for low-bandwidth active suspension systems," *IEEE/ASME Trans. Mechatronics*, vol. 20, no. 5, pp. 2299–2310, Oct. 2015.
- [29] M.Q. Nguyen, M. Canale, O. Senane, and L. Dugard, "A model predictive control approach for semi-active suspension control problem of a full car," in *Proc. IEEE Conf. Decis. Control*, 2016, pp. 721–726.
- [30] L. Xu, H. E. Tseng, and D. Hrovat, "Hybrid model predictive control of active suspension with travel limits and nonlinear tire contact force," in *Proc. Amer. Control Conf.*, 2016, pp. 2415–2420.
- [31] K. Çalışkan, R. Henze, and F. Küçükay, "Potential of road preview for suspension control under transient road inputs," *IFAC Proc.*, vol. 49, no. 3, pp. 117–122, 2016.
- [32] A. Bemporad, M. Morari, V. Dua, and E.N. Pistikopoulos, "The explicit solution of model predictive control via multiparametric quadratic programming," in *Proc. Amer. Control Conf.*, 2000, vol. 2, pp. 872–876.
- [33] A. Bemporad, F. Borrelli, and M. Morari, "Model predictive control based on linear programming – The explicit solution," *IEEE Trans. Autom. Control*, vol. 47, no. 12, pp. 1974–1985, Dec. 2003.
- [34] F. Borrelli, M. Baotic, J. Pekar, and G. Stewart, "On the computation of linear model predictive control laws," *Automatica*, vol. 46, no. 6, pp. 1035–1041, 2010.
- [35] M. Kvasnica, B. Takács, J. Holaza, and S. Di Cairano, "On region-free explicit model predictive control," in *Proc. IEEE Conf. Decis. Control*, 2015, pp. 3669–3674.
- [36] N. Giorgetti, A. Bemporad, and H. E. Tseng, "Hybrid model predictive control application towards optimal semi-active suspension," *Int. J. Control*, vol. 79, no. 5, pp. 521–533, 2006.
- [37] L.H. Csekő, M. Kvasnica, and B. Lantos, "Analysis of the explicit model predictive control for semi-active suspension," *Periodica Polytechnica Elect. Eng.*, vol. 54, no. 1-2, pp. 41–58, 2010.
- [38] M. Canale, M. Milanese, C. Novara, and Z. Ahmad, "Semi-active suspension control using "Fast" model predictive techniques," *IEEE Trans. Control Syst. Technol.*, vol. 14, no. 6, pp. 1034–1046, Nov. 2006.
- [39] T. Paschedag, A. Giu, and C. Seatzu, "Constrained optimal control: An application to semiactive suspension systems," *Int. J. Sys. Sci.*, vol. 47, no. 7, pp. 797–811, 2010.
- [40] J. Theunissen *et al.*, "Explicit model predictive control of active suspension systems," in *Proc. Int. Conf. Adv. Veh. Powertrains*, 2017, pp. 1–19.
- [41] G. Montanez, D. Patino, and D. Mendez, "Comparison of model predictive control techniques for active suspension," in *Proc. Int. Conf. Appl. Electron.*, 2015, pp. 157–160.
- [42] W.F. Milliken and D.L. Milliken, *Race Car Vehicle Dynamics*, Warrendale, PA, USA: SAE Int., 1995.
- [43] S. Fallah, A. Sorniotti, and P. Gruber, "A novel robust optimal active control of vehicle suspension systems," *IFAC Proc.*, vol. 47, no. 3, pp. 11213–11218, 2014.
- [44] D. Hrovat, "Survey of advanced suspension developments and related optimal control applications," *Automatica*, vol. 33, no. 10, pp. 1781–1817, 1997.
- [45] J. Drgona, M. Klauco, F. Janeczek, and M. Kvasnica, "Optimal control of a laboratory binary distillation column via regionless explicit MPC," *Comput. Chem. Eng.*, vol. 96, pp. 139–148, 2017.
- [46] C. Jablonowski, V. Underberg, and M. Paefgen, "The chassis of the all new Audi Q7," in *Proc. 6th Int. Munich Chassis Symp.*, 2015, pp. 37–49.

- [47] M. Anderson and D. Harty, "Unsprung mass with in-wheel motors - myths and realities," in *Proc. 10th Int. Symp. Adv. Veh. Control*, Loughborough, U.K., Aug. 22–26, 2010, pp. 261–266.
- [48] *Mechanical Vibration - Road Surface Profiles - Reporting of Measured Data*, ISO 8608:2016, 2016.
- [49] M. Kvasnica, "Multi-Parametric Toolbox 3," [Online]. Available: <http://people.ee.ethz.ch/~mpt/3/>. Accessed: Jul. 12, 2019.
- [50] D.Q. Mayne, J.B. Rawlings, C.V. Rao, and P.O. Scokaert, "Constrained model predictive control: Stability and optimality," *Automatica*, vol. 36, no. 6, pp. 789–814, 2000.
- [51] D. Karnopp, M.J. Crosby, and R.A. Harwood, "Vibration control using semi-active force generators," *J. Eng. Ind.*, vol. 96, no. 2, pp. 619–626, 1974.
- [52] *Mechanical Vibration and Shock - Evaluation of Human Exposure to Whole-Body Vibration - Part 1: General Requirements*, ISO 2631-1, 1997.



Johan Theunissen received the M.Sc. degree in electro-mechanical engineering from the K.U. Leuven, Leuven, Belgium, in 2008, and the Ph.D. degree in automotive engineering from the University of Surrey, Guildford, U.K., in 2019.

He recently founded Simmanco, an engineering company focusing on mechatronics and automotive. Earlier in his career, he worked for Ford Motor Company, Flanders' DRIVE and Tenneco Automotive Europe, as a Project Engineer and a Project Manager.



Aldo Sorniotti (M'12) received the M.Sc. degree in mechanical engineering and the Ph.D. degree in applied mechanics from the Politecnico di Torino, Turin, Italy, in 2001 and 2005, respectively.

He is a Professor in Advanced Vehicle Engineering with the University of Surrey, Guildford, U.K., where he coordinates the Centre for Automotive Engineering. His research interests include vehicle dynamics control and transmission systems for electric and hybrid electric vehicles.



Patrick Gruber received the M.Sc. degree in motorsport engineering and management from Cranfield University, Cranfield, U.K., in 2005, and the Ph.D. degree in mechanical engineering from the University of Surrey, Guildford, U.K., in 2009.

He is a Reader in advanced vehicle systems engineering with the University of Surrey. His research interests include vehicle dynamics and tire dynamics with special focus on friction behavior.



Saber Fallah received the B.Sc. degree from the Isfahan University of Technology, Isfahan, Iran, in 2001, the M.Sc. degree from Shiraz University, Shiraz, Iran, in 2004, and the Ph.D. degree from Concordia University, Montreal, QC, Canada, in 2010, all in mechanical engineering.

He is a Senior Lecturer of Vehicle and Mechatronic Systems with the University of Surrey, Guildford, U.K. His research interests include vehicle dynamics and control, electric and hybrid electric vehicles, intelligent vehicles, and vehicle system design and integration.



Marco Ricco received the M.Sc. degree in mechanical engineering from the Politecnico di Torino, Turin, Italy, in 2018. He is currently working toward the Ph.D. degree in automotive engineering with the University of Surrey, Guildford, U.K.

His research interests include electric vehicles, vehicle dynamics and vehicle testing.



Michal Kvasnica received the Diploma in process control from the Slovak University of Technology (STUBA), Bratislava, Slovakia, in 2000, and the Ph.D. degree in electrical engineering from the Swiss Federal Institute of Technology, Zurich, Switzerland, in 2008.

He is an Associate Professor (docent) of Automation with STUBA. His research interests include decision making and control supported by artificial intelligence, embedded optimization and control, security and safety of cyber-physical systems, and control of human-in-the-loop systems.



Miguel Dhaens received the M.Sc. degree in electro-mechanical engineering from KIH, Ostend, Belgium.

He is Engineering Manager of the Global Research Ride Performance Team of Tenneco, and responsible for defining the research road map and coordinating the global research activities of Tenneco's Ride Performance business, which includes vehicle dynamics, damping solutions, mechatronics, material science, manufacturing technologies and predictive tools. Before joining Tenneco, he worked with the Formula One team of Toyota Motorsport GmbH, Germany, as Manager of the engine, testing and advanced strategies teams, and with Flanders' DRIVE as R&D Manager.